The EUV Solar Irradiance Spectrum Observed with the Coronal Diagnostic Spectrometer (CDS) on SOHO

P.Brekke

ESA Space Science Department, NASA Goddard Space Flight Center, Code 682.3, Greenbelt, MD 20771, USA

W. T. Thompson

SM&A Corporation, Space Sciences Division, 9315 Largo Dr. West, Largo, MD 20774, USA

T. N. Woods, and F. G. Eparvier

The Laboratory for Atmospheric and Space Physics (LASP), 1234 Innovation Dr, Boulder, CO 80309, USA

Received _____; accepted _____

ABSTRACT

We present a calibrated solar EUV irradiance spectrum in the range 307–380 Å and 515–632 Å. The "*Sun as a Star*" spectrum was recorded by the Coronal Diagnostic Spectrometer (CDS) on SOHO on May 15, 1997 using the normal incidence spectrometer (NIS) with a spectral resolution between 0.3 and 0.6 Å. The relatively high spectral resolution allows the separation of blends and the differentiation of weak emission lines. The full disk spectrum is compared with simultaneous well-calibrated EUV irradiance measurements from a NASA/LASP rocket payload to validate the pre-flight calibration of CDS. Significant errors in the pre-flight calibration were found and a new calibration has been established for the CDS/NIS system.

The present spectrum includes emission lines formed in the temperature range 10^4 to over 10^6 K. Line fluxes for the most prominent lines are extracted for the calibration and for the solar irradiance studies. This measurement should represent well solar minimum conditions as the daily 10.7 cm radio flux was 73 (units of 10^{-22} W m^{-2} Hz^{-1}). A modest spatial resolution, constrained by the observing mode used, allows for the discrimination between quiet and active sun. The calibrated quiet Sun irradiance spectrum is compared with previous measurements.

Subject headings: Sun: atmosphere, Sun: UV radiation, Sun:solar-terrestrial relations, Sun: transition region, Sun: corona, Sun: chromosphere

1. Introduction

The solar extreme ultraviolet (EUV) spectrum at wavelengths below 1200 Å is the dominant source of energy for heating and ionization in the terrestrial upper atmosphere at altitudes above 90 km. A good knowledge of the solar EUV spectral irradiance is thus of critical importance for many analyses of the photochemistry and energy balance planetary atmospheres, the interstellar medium and comets.

Solar measurements in the vacuum ultraviolet (VUV: below 2000 Å) region of the spectrum are only possible above the atmosphere and were first made photographically (e.g., Baum et al., 1946; Behring, Cohen, & Feldman, 1972), and then by photometric detectors, on short duration rocket flights starting after the Second World War. The SOLRAD and AEROS satellites, Air Force Cambridge Research Laboratories rocket experiments, Orbiting Solar Observatory (OSO) 3 and 4, (Hall & Hinteregger, 1970; Reeves & Parkinson, 1970) and Atmospheric Explorer (AE) C, D, and E (Hinteregger et al., 1973) conducted survey observations through different parts of the spectrum during the 1960s and 1970s.

Following the last AE-E measurements in 1981, there has been a long hiatus without routine measurements of the solar EUV irradiance. Some recent progress in making solar EUV irradiance observations includes measurements from the San Marco 5 satellite from March to December 1988 (Schmidtke et al., 1992), a few NASA sounding rocket experiments (e.g., Ogawa & Judge, 1986; Woods & Rottman, 1990; Ogawa et al., 1990; Woods et al., 1998), and now from the SOHO CDS, SUMER and Solar EUV Monitor (SEM) instruments. Some recent reviews of the solar EUV irradiance are given by Lean (1991) and Tobiska (1993).

The spectral resolution for previous solar EUV irradiance measurements is typically 1 to 10 Å. The higher spectral resolution of the SOHO CDS (0.3-0.6 Å) allows for improved separation of blends and differentiation of weak emission lines in the solar spectrum.

Measurements of the solar spectral energy distribution are often divided into two groups. Some instruments use only a spectrometer and observe the spectral irradiance of the integrated solar disk. The irradiance measurements are designed to study the Sun's radiant energy output and its variability and thus, require very high photometric accuracy and instrument stability. Other instruments employ an imaging device followed by the spectrometer and observe the radiance from a limited area of the solar disk. The primary goal with the radiance measurements are to differentiate between various emitting regions on the Sun. However, it is much more difficult to achieve high photometric accuracy because of the more complex optics and the often larger number of reflecting surfaces.

The present high resolution full disk spectrum were obtained with the Coronal Diagnostic Spectrometer (CDS) on SOHO by combining radiance measurements taken over the full disk. These observations are compared with a simultaneous EUV irradiance measurement from a NASA/LASP (Laboratory for Atmospheric and Space Physics) rocket payload to validate the pre-flight calibration of CDS.

Before proceeding we will make explicit our terminology. "Irradiance" is the total flux density of the radiation from the entire solar disk at 1 AU, with units of mW m^{-2} (1 mW m^{-2} = 1 erg cm^{-2} s^{-1}) or ph cm^{-2} s^{-1} as used in this paper. "Radiance" is the specific intensity (mW m^{-2} sr^{-1} or ph cm^{-2} s^{-1} sr^{-1}) of a given resolved feature on the solar disk. We will use the terms "irradiance" and "radiance" hereafter.

2. Instrument and Observations

The CDS telescope is a Wolter-Schwarzschild type 2 design in which the incident beam first makes a grazing incidence reflection off the internal surface of a paraboloid and then another grazing incidence reflection from the external surface of a confocal hyperboloid.

The telescope feeds simultaneously a normal incidence spectrometer (NIS) and a grazing incidence spectrometer (GIS), which share a common slit. The present observations were obtained with NIS, where the beam after a single normal reflection off two toroidal gratings is focused onto an intensified CCD detector. NIS contains two gratings, mounted side by side, with different rulings such that for the same incident and exit angular range they disperse two different wavelength bands, namely 310 - 380 Å and 520 - 630 Å. The astigmatic grazing incidence spectrometer (GIS) covers four wavelength bands in the range 150–780 Å. The observations presented here were made with the normal incidence spectrometer (NIS) on CDS. For a full description for this spectrometer and the CDS instrument in general we refer to Harrison et al. (1995).

The normal incidence spectrometer is stigmatic, providing a focussed image along the length of its entrance slit. Figure 1 shows the spectral 'images' as they appeared on the detector for an active region observation made on March 14, 1997, at 11:03 UT. Two portions of the 1024 × 1024 pixel detector array are shown where each panel represents a plot of wavelength (abscissa) versus spatial position along the spectrometer slit (ordinate). The spatial positions are given in arcseconds from the Sun center. This particular observation was part of a observing program executed regularly to derive spectral atlases of different solar features (the study name is NISAT_S). The $2'' \times 240''$ slit was used; thus one sees a $2'' \times 240''$ image of the Sun dispersed in wavelength space across the two ranges.

One clearly sees a number of emission lines (this is a negative print, thus the lines show up as dark features) and their variation along the slit. Note how some lines (e.g. the strong Fe XVI lines at 335 and 360 Å) are strong at the lower portion of the slit while others (e.g. Mg IX 368 Å and O V 629 Å) are stronger at other locations along the slit. The spatial distribution of emission above active regions as a function of temperature has been discussed in detail by Fludra et al. (1997) and Brynildsen et al. (1997). The

spectra shown in Figure 1 has been processed to remove the cosmic ray interaction with the detector system which shows up as bright dots and short tracks. This is a feature of several of the imaging instruments on SOHO and, in most instances, can be removed by software techniques. Since SOHO is located well outside the magnetosphere such effects were anticipated.

The spectral resolution of the NIS is between 0.3 and 0.6 Å, which is better than most previous irradiance monitors. Various slit widths are available for the NIS. By rastering the instrument, i.e. moving the solar image perpendicular to the slit, the spectrometer builds up images of solar features in a series of spectral lines. In most observing sequences telemetry constraints make it necessary to pre-select a number of wavelength windows from the detector. In Figure 1 the line windows extracted when deriving monochromatic full disk images (see section 2.1) are illustrated. The instantaneous field of view (FOV) of CDS (without repointing the instrument) is $240'' \times 240''$. However, the FOV can be repointed to any position of the Sun as well as outside the limb. Two techniques have been developed to observe the full disk of the Sun both which are discussed below.

2.1. Full disk images

Monochromatic full disk images in a set of emission lines can be derived from a mosaic of 69 different pointings. Each of the 69 "rasters" ($240'' \times 240''$ FOV) is obtained by stepping the $4'' \times 240''$ slit $4''$ between each exposure. Thus, one raster contains 60 exposures each with an integration time of 3 s. A detailed description of the CDS full sun observations is given by Thompson & Carter (1998). Normally 6 pre-selected wavelength windows, centered on a set of strong emission lines, are extracted from the detector (see Figure 1 and Table I). The onboard compression consists of summing up all counts along the direction of dispersion in each line window. Thus, for each slit position the total counts

in the line at each spatial position along the slit is transmitted. Using this compression scheme the spectral information (the shape of the line profiles) is lost. By building up monochromatic images CDS is able to distinguish differences in the emitting plasma on a finer graded temperature scale compared to instruments which make use of broad band filters (e.g. Extreme ultraviolet Imaging Telescope - EIT and Yohkoh). Full disk images are usually obtained once every month as part of the CDS synoptic program.

The images cover temperatures between 2×10^4 K and 2.5×10^6 K. Thus the CDS observations form a complementary set of full diks images to those of EIT by filling in the gap between 5×10^4 K and the hotter lines seen by EIT. In addition CDS includes even hotter Fe XVI 335 Å line in active regions. Selected monochromatic full disk images obtained on May 16, 1997 are shown in Figure 2 and illustrate the features contributing to the full disk flux from the Sun at different temperatures. As can be seen from the full disk images a few small active regions and bright points are visible at the time of this particular observation. The network structure is clearly visible in He II 304 Å (6×10^4 K), and O V 629 Å (2.5×10^5 K), while in the Mg IX 368 Å (9.5×10^5 K) image the network pattern is less apparent. In the Fe XVI 335 Å (2.5×10^6 K) image the emission comes from the active regions and bright compact regions.

Although the monochromatic images are built up from a large number of exposures all the lines are observed simultanously in each exposure. This allows direct comparison with other lines at the same spatial location. The dark vertical lines are loss of data during the realtime transmission.

2.2. Full disk spectrum

To derive the full disk irradiance spectrum the same 69 different pointings of the CDS FOV were required to cover the entire Sun. However, to derive the flux over the entire NIS wavelength range it was necessary to both do onboard compression and to undersample the Sun during the rastering of the slit. The undersampling was accomplished by stepping the $4'' \times 240''$ slit $24''$ between each exposure. Thus only 10 exposures were obtained within each FOV pointing which reduced the total duration of the observing sequence from 72 hours to 12 hours. The onboard compression scheme is to sum up all the intensities along the $240''$ slit resulting in a 1 dimensional spectrum for each exposure. The final reduction includes applying the flat-fielding and calibration (see section 3) before adding up all the spectra from the 69 FOV pointings taking into account the undersampling of a factor 6.

An important consideration is whether or not the undersampling affects the accuracy of the irradiance measurement. To test this, we analyzed image data of the full Sun similar to that shown in Figure 1, to see what the effect of undersampling by various factors would have on the derived flux. This effect was found to be very small, on the order of 1%, for most lines. There is still a concern that lines which originate from compact regions on the sun, such as the very hot Fe XVI lines at 335 and 361 Å, may have a larger error associated with them.

The full disk spectrum obtained on May 15 1997 is shown in Figure 3 with the identification of the brightest emission lines. The identifications were adopted from Harrison (1993), the Chianti line list (Dere et al., 1996) and a recent line list based on CDS quiet Sun observations (Brooks et al 1999). The wavelength range between 510-633 Å is dominated by the He I 584 Å line as well as bright lines from O III, O IV, O V, and Mg X. In addition the He II 304 Å line shows up in second order around 608 Å. This wavelength band contains an enormous spread of temperatures and well separated, bright lines, useful for dynamic

studies throughout the transition region and corona. The shorter wavelength range (310-380 Å) is more complex and is dominated by Mg IX 368 Å and a number of lines from highly ionized ions, in particular iron. The spectral resolution performance of NIS is illustrated in Figure 4 which shows expanded wavelength plots of selected emission features.

Measurements of the CDS/NIS gratings prior to integration into the instrument showed that the measured spectra would be subject to contamination from light at wavelengths outside the desired band. Laboratory measurements were made at 1236 Å, close to that of the strong Lyman α line at 1216 Å, and demonstrated that this radiation showed up as a roughly constant signal in both spectral bands. Superimposed as a dotted line in each graph in Figure 3 is the effect that a constant background would have on the two spectra, after passing through the calibration process. One can readily see that these curves match the observed backgrounds quite closely, confirming the hypothesis of off-band scattering. Possible sources of this contamination are Lyman α and the Lyman continuum. Before these data can be compared against other observations, the estimated background in the CDS data must be removed.

3. Instrument Calibration

To be able to determine the solar EUV irradiance as well as derive diagnostic information on the plasmas of the solar atmosphere, an accurate knowledge of the instrument sensitivity (photons detected by the instrument per solar photons) is essential. Absolute intensities and intensity ratios can be used to obtain information of density, temperature and abundances. Even if instruments with improved spectral, spatial and temporal resolution has been developed during the last decades the photometric accuracy has not seen the same development. Typical accuracies in published UV spectral data are still on the order of 25–50%. In addition the stability of the radiometric calibration

of any EUV instrument is a concern based on the experiences with previous solar EUV missions, which suffered from serious sensitivity degradation during their operation under solar irradiation. Below we discuss different aspects regarding the instrument calibration before and after the launch of SOHO.

The normal incidence detector of CDS consists of a windowless microchannel plate (MCP) intensifier tube that detects and converts the EUV radiation to electrons, which are intensified, and then converted to visible light via a standard P-20 phosphor coated on the fiber-optic output window. The visible light is focused via a lens and is recorded by a 1024×1024 charge coupled device (CCD). For a more detailed description of the detector see Harrison et al. (1995). The raw data from the CDS NIS detector is in Analog to Digital Conversion units. Converting this into physical units is a three step process. The first step is to remove the CCD readout bias, which is separately measured for each exposure. After this, the second step is to apply the wavelength-independent calibration parameters peculiar to the detector, including the exposure time, the MCP amplification, and a flat-field correction. Once this step is applied, the units of the data are photon-events/pixel/s. Here the term photon-events refers to the photons which have actually been detected by the instrument, as opposed to the photons which impinge on the detector. The final step in calibrating is to convert the photon events into absolute radiance units. This includes the following factors: 1) the quantum efficiency of the NIS detector, 2) the wavelength calibration of the NIS spectrograph, which determines how to apply the quantum efficiency parameters, and 3) the effective area of the CDS telescope and NIS spectrograph. Note that the calibration depends on the slit used to make the observation.

Included in the flat-field correction is a correction for differential aging of those parts of the MCP which are most exposed to light. The bulk of NIS measurements are made with either the $2'' \times 240''$ slit or the $4'' \times 240''$ slit. Since there is no wavelength selection

mechanism on CDS, emission lines always fall on the same detector pixels. Those detector pixels which are exposed to strong emission lines will age more quickly than other pixels. The lines become "burned-in". The amount of aging can be measured by opening up the aperture to $90'' \times 240''$ and looking at the profiles. Locations where the strong spectral lines have aged the detector will appear as depressions in the profile. Observing at several quiet sun locations averages out solar features which may confuse the measurement. It is a regular part of the CDS synoptic program to measure these burn-in areas several times per week. No attempt has been made to correct for any possible loss of sensitivity from the less frequently used $90'' \times 240''$ slit, which cannot be directly measured in the same way as the narrow slit burn-in. Thus, the calibration curve derived here is correct only for the observation date of 15 May 1997. However, it is expected that this additional correction should be relatively small in May of 1997, expect possibly around the very strong He I 584 Å line.

The preflight calibration of the CDS instrument (Bromage et al. 1996 and Lang et al. 1999) was performed using an absolute EUV radiation source (Hollandt et al., 1994) which was calibrated directly against the BESSY synchrotron beam. The currently assumed wavelength dependence was derived from the analysis of density insensitive line ratios (Pike 1996 and Landi et al. 1997).

3.1. Underflight Calibration Experiment

There have been attempts to calibrate the CDS instrument using several different rocket payloads. The approach used in this work was to compare the CDS full disk measurements with simultaneous well calibrated EUV irradiance measurements from a NASA/LASP rocket payload.

The NASA/LASP rocket experiment includes several solar EUV instruments (Woods et al., 1994a). The solar EUV irradiance for the SOHO CDS calibrations is from the EUV Grating Spectrograph (EGS), which is a prototype instrument for the NASA Thermosphere Ionosphere Mesosphere Energetic Dynamics (TIMED) mission (Woods et al., 1994b). The EGS is a normal-incidence 1/4 m Rowland circle spectrograph. The EGS spectral coverage is 250 to 1950 Å with a 1.67 Å bandpass per anode on the array detector; thus the realistic spectral resolution is 4.5 Å. The grating is a 600 lines per mm ruled grating from Hyperfine with a gold coating to maximize the efficiency at the shortest wavelengths. The array detector is the 64 x 1024 CODACON array detector developed by Dr. George Lawrence at LASP (McClintock et al., 1982). The CODACON detector uses microchannel plates (MCPs) and coded anode electronics for its readout. Each detector anode (pixel) is 25 μm wide (dispersion direction) by 100 μm long. The EGS is calibrated using the Synchrotron Ultraviolet Radiation Facility (SURF) at the National Institute of Standards and Technology (NIST) in Gaithersburg, Maryland (Parr & Ebner, 1987). The algorithms for converting the EGS data to irradiances are given by Woods & Rottman (1990) and Woods et al. (1998). The uncertainty for the EGS measurements, which is wavelength dependant, is estimated to be 20% in the NIS1 wavelength band and 12% in the NIS2 band.

3.2. Comparison of CDS irradiance with rocket data

Comparing two different measurments of the EUV irradiance is not straight forward. The simplest method would be to degrade the CDS spectrum to match the spectral resolution of EGS. We tried this method but it did not work very well. One of the problems was disentangeling differences in the two spectra due to the background from differences due to a wavelength dependent calibration curve. Using this technique we were unable to derive a unique result. Another method was used where these effects were decoupled from

each other as described below.

The CDS irradiance is compared with the sounding rocket observations in Figures 5 and 6 (upper panels) where the different spectral resolutions are apparent. The CDS observations can be characterized as consisting of distinct spectral lines on top of a slowly varying background which is primarily instrumental in origin. One way to remove the effect of the background component is to fit sections of the spectrum as a sum of a series of Gaussian line profiles together with a polynomial representing the local background. The total intensity within a spectral region can then be modeled as the sum of the areas under the Gaussian profiles. This technique was applied to six regions in the long wavelength channel of the CDS Normal Incidence Spectrograph (NIS2), where the lines form natural groups which are easily distinguished in the sounding rocket data. The region around 608 Å was not analyzed because of contamination from second order 304 Å radiation in both spectrographs.

The rocket intensities in the same regions were derived in two ways. One way was to simply sum together the intensities in the bins making up the line group. The second technique differed from the first in that the bin intensities on either side of the line group were interpolated and subtracted from the summed bins. This was an attempt to account for any residual instrumental background in the sounding rocket data, and as such represents a kind of lower limit (aside from other uncertainty considerations) for the rocket intensities. In both cases, an adjustment of $\sim$2% was made to account for the fact that SOHO is closer to the Sun than the Earth.

The result of dividing the rocket intensities into the CDS intensities is shown in Figure 6 (lower panel). The solid lines represent the ratio with no adjustment for background in the rocket data, and the dashed lines represent the case where the bins between line groups are used to estimate a presumed background. The difference between the two

techniques is an indication of the reliability of the results. The cross in each bin shows the average wavelength weighted by line intensity. The ratio shown in Figure 6 represents a correction factor which needs to be applied to the presumed CDS sensitivity curve. For example, at 584 Å, the ratio is approximately 1.6. This means that the CDS sensitivity was underestimated by a factor of 1.6 at this wavelength. It appears that little correction needs to be applied to the shape of the original calibration curve between about 540 and at least 590 Å. The downturn in the ratio below 530 Å is somewhat problematical because the lines there are weaker than in other parts of the spectrum. More confidence can be placed in the upturn at the long wavelength end. The region between 590 and 600 Å proved to be particularly difficult to fit, and that data point is not used in the subsequent analysis.

Figure 7 shows the effect of the correction factor derived above on the original CDS calibration. The dot-dashed line is the original calibration curve. It can be expressed by the equation

$$\epsilon = 0.00165948 - (2.34540 \times 10^{-6})\lambda \quad (1)$$

where ϵ is the instrument sensitivity, defined as the number of photons which interact with the detector (photon-events) divided by the total number of photons. The product of the correction factors from Figure 6 and Equation 1 is shown as solid or dashed lines, where the line styles and symbols have the same meaning as in Figure 6. The dotted line shows a smooth curve selected to pass through all the regions between the solid and dashed lines, but without attempting to replicate all the downturn at the short wavelength end. The equation for this modified calibration curve is

$$\epsilon = -0.079766523 + (0.00042961647)\lambda - (7.6058825 \times 10^{-7})\lambda^2 + (4.4558175 \times 10^{-10})\lambda^3 \quad (2)$$

Taking the rocket calibration of ∼12% in this wavelength region into account, the uncertainty associated with Equation 2 varies from 15% near the 584 Å line to 25% at either end of the spectrum. It should be emphasized that the CDS calibration derived here

characterizes the instrument behavior as of 15 May 1997, when the CDS and EGS sounding rocket irradiances were measured. Although a correction was applied for the burned in slit profiles on the CDS detector, there may be other sources of detector sensitivity changes prior to that date which are not accounted for. In particular, the instrument sensitivity may be affected by occasional solar exposure through the 90″ wide imaging slit. Note that the data points in Figure 7 at 584 Å fall somewhat below the fitted curve. This may be evidence for some sensitivity loss in the area around this very strong line, while other areas are less affected.

The situation with the short wavelength channel, NIS1, is less clear, as shown in Figure 5 (top panel). Here the lines are more closely spaced, and the only really strong line is at 368 Å. The ratio of the irradiances derived from CDS to the rocket data, shown in the bottom panel of Figure 5, has much higher scatter as a result. Deriving a correction to the wavelength dependence from these data is not really possible. However, a single correction value of 2.3 passes between the solid and dashed lines in all wavelength regions, as is demonstrated by the dotted line in Figure 5. Folding in the rocket uncertainty of ∼20% for this wavelength region, the uncertainty of the corrected calibration must be considered to be 45% almost everywhere except very close to the 368 Å line, where it drops to 25%.

These results support other work which conclude that the original CDS calibration underestimated the NIS sensitivities. Lang et al. (1999) re-examined the preflight NIS laboratory measurements and derived a higher NIS2 sensitivity at 584Å than the original calibration would imply. The amount of adjustment is similar to the value derived here. Landi et al. (1997) used DEM analysis to examine the relative calibration of NIS1 to NIS2, and concluded that the NIS1 to NIS2 sensitivity ratio was underestimated by a factor of 2.5–5. We also derive that the NIS1 to NIS2 sensitivity ratio is underestimated, but only by a factor of ∼1.4 over most of the spectrum.

Since the EGS sounding rocket measurements included 304 Å in first order, it is also possible to characterize the CDS second-order calibration at 2×304 Å. In the CDS spectrum, the He II line at 303.8 Å can be separated from the Si XI line at 303.3 Å, while in the EGS spectrum, the combined intensity of the two lines can be extracted. To match the EGS measurements, the CDS second-order sensitivity at 304 Å must be 1.64×10^{-5}, with an uncertainty of 20%, based primarily on the uncertainty of the rocket measurements. Again, this is higher than the value of 1.32×10^{-5} based on the preflight measurements (Lang et al. 1999).

4. The Quiet Sun Spectrum

From the above discussion we argue that there are significant errors in the preflight calibration of CDS and by comparing our measurments to the EGS spectrum we have established a new calibration for the CDS NIS system. In Table II we present the observed line fluxes for the most prominent emission lines (Brooks et al. 1999) in the CDS spectral range based upon this new calibration. The values have been derived from Gaussian fits to the line profiles with the background subtracted. The line fluxes have furthermore been adjusted according to the correction factors found from the comparison between CDS and the rocket measurements. The values in Table II are reported at SOHO's position, which on 15 May 1997 was at almost exactly 1 A.U. from the Sun. The flux values should represent well solar minimum conditions as the daily 10.7 cm radio flux was 73 (units of 10^{-22} W m^{-2} Hz^{-1}). Together with the fluxes, we present two measures of the uncertainty associated with the measurements. The first, labeled "Stat. σ", is the statistical uncertainty of the intensity from the Gaussian fitting process. The second, labeled "Total σ", is the combined total, in the root-summed-squares sense, of the statistical uncertainty from the fit, the counting statistics from the number of photons collected (a small contribution), and the

estimated uncertainty in the calibration. Wavelengths are based on Brooks et al., 1999, except for the two Fe XVI lines which are based on Kelly, 1997. Some lines which were separated in Brooks et al. are here blended, at 359.7, 539.6, and 554.5 Å. These blends are noted in Table II. We also report the Si X line at 621.1 Å, which was not seen in the quiet Sun spectra analyzed by Brooks et al.

When deriving the line fluxes care has been taken to also differentiate obvious blends. Some lines listed in Table II still include contributions from blends as noted in the right column. Problems associated with blended lines in the CDS NIS spectrum have been discussed by Mason et al (1997) and Brekke et al. (1997).

5. Comparison with previous reference spectra

We have compared our calibrated irradiance spectrum with the AE-E quiet Sun reference spectrum SC21REFW (Hinteregger et al., 1981) and associated model based on the daily and 81-day average F10.7 radio flux on May 15, 1997. Because the Sun was so close to solar minimum, the difference between the model and the reference spectrum is small. Figure 8 shows the comparison between the Hinteregger et al. (1981) model, and the irradiances as measured by CDS. The model predicts generally lower irradiances than those observed for the CDS short wavelength channel (NIS-1), and generally higher irradiances for the long wavelength channel (NIS-2). The differences can be as high as a factor of two. In the short wavelength channel, when comparing individual lines, the modeled irradiance is generally higher than the measured irradiance. However, the measured integrated irradiance is higher than predicted by the model. This is because the irradiances measured by CDS include many more lines than those accounted for in the model.

When the Hinteregger et al. (1981) model is integrated over the entire NIS-1 bandpass

of 310–380 Å, the total predicted irradiance of 2.04×10^9 ph cm^{-2} s^{-1} agrees much better with the measured irradiance of 2.24×10^9 ph cm^{-2} s^{-1}. However, the model prediction for the total integrated NIS-2 bandpass of 510–630 Å is significantly higher than that measured by CDS (5.51×10^9 vs. 3.65×10^9 ph cm^{-2} s^{-1}). Since the NIS-1 bandpass is dominated by coronal lines, while the NIS-2 bandpass is dominated by chromospheric and transition region lines, this may indicate that the Hinteregger et al. (1981) model is better at predicting the coronal contribution to the total irradiance than the chromospheric and transition region contribution, when the solar activity is close to minimum or for this particular day.

The differences shown in Figure 8 are consistent with a comparison by Woods et al. (1998) of several EGS rocket measurements to the models by Hinteregger et al. (1981), Tobiska & Eparvier (1996), and Richards et al. (1994). A comparison to the Donnelly & Pope (1973) reference spectrum also revealed factor of 2 differences when compared with similar levels of activity. Woods et al. (1998) argued that while solar variability can explain some of these differences, instrument calibration errors for the earlier experiments may be the prime contribution to the differences.

Thus, the more accurate sounding rocket measurements, which were used as the basis of the CDS calibration, suggest a revision of the previous AE-E reference spectrum, as well as the models which are based upon this data set.

6. Comparing irradiance and disk center radiance

It is not straightforward to compare irradiance measurements and spatially resolved radiance values. A detailed knowledge of the center-to-limb variation of each spectral feature is required as well as an estimate of the contribution from active regions and other

bright compact features. However, to illustrate the effects of the presence of active regions as well as the center-to-limb variation of the different emission features we do the following exercise. The full-disk-flux measured at Earth from an emission line at wavelength λ is related to the quiet Sun radiance by the relations

$$F_{qs}(\lambda) = \frac{2\pi R_{\odot}^2}{R^2} \langle I_{qs}(\lambda) \rangle, \tag{3}$$

(e.g. Warren, Mariska, & Lean 1998). Here $R_{\odot}$ is the solar radius, R is the distance between the Sun and the Earth, and $\langle I_{qs}(\lambda) \rangle$ is the disk-averaged radiance:

$$\langle I_{qs}(\lambda) \rangle \equiv 2 I_{qs}(\lambda) \int_0^{\infty} E_{\lambda}(r) r \, dr. \tag{4}$$

Here $I_{qs}(\lambda)$ is the specific radiance at disk center and

$$E_{\lambda}(r) \equiv \frac{I_{qs}(\lambda, r)}{I_{qs}(\lambda)} \tag{5}$$

parameterize the center-to-limb variation of the radiance where r is the radial polar coordinate.

The average radiance at disk center was derived from the raster obtained at disk center and converted to irradiance using the above relation. As can be seen from the full disk images this area represents a fairly quiet Sun. The "disk average" irradiance is compared to the true full Sun irradiance in Figure 9. As can be seen some line ratios are different in the two spectra—in particular the Fe XVI lines (335 Å and 360 Å), which are absent in the quiet Sun spectrum while strong in the full disk spectrum. This is mainly due to the contribution from the active regions (see Figure 2) as well as the limb brightening of the hotter coronal and transition region lines. It should be noted that Fe XVI 335 Å is blended

with a quiet Sun line (Mg VIII 335.3 Å) as reported by Brekke et al. (1997). Thus, the emission seen at this wavelength in the upper plot is almost entirely due to the Mg VIII emission.

7. Summary

We have presented a calibrated high resolution EUV irradiance spectrum in the wavelength ranges 310–380 Å and 520–630 Å. The observations were obtained as part of a *SOHO Intercalibration Joint Observing Program* (No. 011) where several SOHO instruments participated together with two full disk irradiance monitors. The EUV irradiance was observed from a NASA/LASP rocket payload which covered the spectral range from 250 to 1950 Å with 4.5 Å spectral resolution. This instrument was radiometrically calibrated at NIST/SURF. The primary objective of the irradiance instrument for this flight was to obtain a radiometrically calibrated "typical" solar minimum full disk EUV solar spectrum. However, the rocket flight also provided an unique opportunity to validate the pre-calibration of the CDS instrument. Significant errors in the pre-flight calibration were found and a new calibration has been established for the CDS/NIS system.

The present work has demonstrated that the CDS instrument can be used to build up "Sun as a Star" spectra which can be compared with other irradiance observations as well as stellar EUV data. CDS is currently monitoring the EUV spectral irradiance on a regular basis and will add valuable information about the variation of the EUV output from the Sun as we approach solar maximum, in particular since there are no other regular observations of the EUV spectral irradiance at present. We plan a follow up paper on the analysis of irradiance variations obtained with CDS since 1997. In addition to the irradiance measurements, CDS also produces monochromatic images in selected lines once a month as part of the synoptic observing program. The combination of the CDS images

and the full-disk solar irradiance measurements makes it possible to quantify the important sources of the irradiance variability. The relatively high spectral resolution will in addition give detailed information of the contribution to the EUV irradiance that illuminates the upper atmosphere of the Earth.

While FSUN is executed once every month, another smaller synoptic observing sequence (SYNOP) is taken every day. A 4 arc minute wide north-south scan, centered on the central meridian has been designed to monitor the global evolution and structure of the Sun. It allows a thorough study of the stability and evolution of large-scale features in conjunction with coronagraphs (LASCO, UVCS) and full-Sun detectors (EIT, Yohkoh, GOES, and ground based observations). Since a feature on the solar disk (close to the central meridian) rotates approximately 3.6 arcmin in one day the CDS scans will provide a complete coverage. Thus, Carrington rotation maps can be derived, allowing for the monitoring of long-term variations in the solar irradiance.

We would like to thank our many colleagues in the CDS consortium in the UK, Germany, USA, and Norway, who have made CDS into such an excellent instrument and provided operational and data reduction software support. This work was supported by The Research Council of Norway, and by NASA Grant NAS5-32350. SOHO is a project of international cooperation between ESA and NASA. The NASA/LASP rocket program is supported by NASA Grant NAG5-5141, and the TIMED SEE EGS instrument used on this rocket flight is supported by NASA/JHU APL Contract JH-774017.

REFERENCES

Baum, W. A., Johnson, F. S., Oberly, J. J., Rockwood, C. C., Strain, C. V., & Tousey, R.: 1946, Phys. Rev., 70 781

Behring, W. E., Cohen, L., & Feldman, U.: 1972, ApJ, 175, 493

Brekke, P., Kjeldseth-Moe, O., Brynildsen, ., Maltby, P., Haugan, S. V. H., Harrison, R. A., Thompson, W. T., & Pike, C. D. 1997, Sol. Phys., 170, 163

Bromage, B. J. I., Breeveld, A. A., Kent, B. J., Pike, C. D., & Harrison, R. A.: 1996, University of Central Lancashire report CFA/96/09.

Brooks, D.H., Fischbacher,G.A., Fludra, A., Harrison, R.A., Innes, D. E., Landi, E., Landini, M., Lang, J., Lanzafame, A.C., Loch,S.D., McWhirter, R.W.P., Summers, H.P., & Thompson, W.T. 1999, A&A347, 277.

Brynildsen, N., Brekke, P., Fredvik, T., Haugan, S.V.H. Kjeldseth-Moe, O., Maltby, P., Harrison, R.A., Pike, C.D., Rimmele, T., Thompson, W.T., & Wilhelm, K. 1998 Sol. Phys., 179, 43.

Dere, K. P., Landi, E., Mason, H. E., Monsignori Foss, B. C, & Young, P. R. 1997, A&AS, 125, 149.

Donnelly, R. F., & Pope, J. H. 1973, Tech. Repl. ERL 276-SEL 25, NOAA, Boulder

Fludra, A., Brekke, P., Harrison, R. A., Mason, H. E., Pike, C. D., Thompson, W. T., & Young, P. R.: 1997, Sol. Phys., 175, 487.

Hall, L. A., & Hinteregger, H. E. 1970, J. Geoph. Res., 75, 6959

Harrison et al.: 1995, Sol. Phys., 162, 233

Harrison : 1993, The Coronal Diagnostic Spectrometer for SOHO, The CDS Blue Book

Hinteregger, H. E., Bedo, D. E. & Manson, J. E. 1973, Radio Science, 8, 349

Hinteregger, H. E., Fukui, K. & B. R. Gilson,B. R. 1981, Geophys. Res. Lett., 8, 1147

Hollandt et al. 1994, Appl. Opt.33, 68

Kelly R. L., 1987, J. Phys. Chem. Ref. Data 16, Suppl. 1.

Landi, E., Landini, M., Pike, C.D. & Mason, H.E., 1997, Sol. Phys., 175, 553.

Lang, J., Kent, B. J., Breeveld, A. A., Breeveld E. R., Bromage, B. J. I., Hollandt, J., Payne, J., Pike, C. D., & Thompson, W. T., Rutherford Appleton Laboratory Technical Report RAL-TR-1999-036.

Lean, J. 1991, Rev. of Geophys., 29, 505

Mason, H.E., Young, P. R., Pike, C. D. Harrison, R. A., Fludra, A., Bromage, B. J. I., & Del Zenna, G. 1997, Sol. Phys., 170, 143

McClintock, W. E., Barth, C.A., Steele, R.E., Lawrence, G.M., & Timothy, J.G. 1982, Appl. Opt., 21, 3071

Ogawa, H. S. & D. L. Judge,D. L. 1986, J. Geophys. Res., 91, 7089

Ogawa, H. S., Canfield,L. R., McMullin, D., & Judge, D. L. 1990, J. Geophys. Res., 95, 4291

Parr, A. C. & Ebner, S. 1987, SURF II User Handbook, NBS Special Publication, Gaithersburg, MD

Pike, C. D.: 1996, private communication

Reeves, E. M. & W. H. Parkinson, W. H. 1970, ApJS181, 1

Richards, P. G., Fennelly, J. A., Torr, D. G. 1994, J. Geophys. Res., 98, 10,667

Schmidtke, G., Woods,T. N., Worden, J., Doll, H., Solomon, S. C., & Rottman,G. J. 1992, Geophys. Res. Lett., 19, 2175

Thompson, W., & Carter, M. 1998, Sol. Phys., 178, 71.

Tobiska, W. K. & Eparvier, F. 1996, Sol. Phys., 177, 147

Tobiska, W. K. 1993, J. Geophys. Res.., 98, 18,897

Warren, H. P., Mariska, J. T., & Lean, J. 1998, J. Geophys. Res., 103, 12091

Woods, T. N., Rottman, G. J., Bailey, S. M., Solomon, S. C., & Worden, J. R. 1998, Sol. Phys., 177, 133

Woods, T. N., Rottman, G. J., Bailey, S., & Solomon, S. C. 1994a, Optical Eng., 33, 438

Woods, T. N., Rottman, G. J., Roble,R. G., White, O. R., Solomon,S. C., Lawrence, G. M., Lean,J., & Tobiska, W. K. 1994b, SPIE Proceedings, 2266, 467

Woods, T. N. & G. J. Rottman, G. J. 1990, J. Geophys. Res., 95, 6227

This manuscript was prepared with the AAS LaTeX macros v4.0.

Table 1: Emission lines used for synoptic full disk images

Ion	Wavelength [Å]	Temp. of formation [K]
He I	584.33	2.0×10^4
He II	2×303.78	4.6×10^4
O IV	554.52	1.7×10^5
O V	629.73	2.3×10^5
Mg IX	368.06	9.5×10^5
Fe XVI	335.40	2.7×10^6

Table 2. Observed Solar EUV Irradiance [ph cm^{-2} s^{-1}] at SOHO (1 A.U.)

Ion	λ_{ref} Å	Flux	Stat. σ 10^7 ph cm^{-2} s^{-1}	Total σ	Remarks
Mg VIII	313.758	5.79	1.18	2.86	
Si VIII	314.378	6.22	1.27	3.07	
Mg VIII	315.019	11.38	0.70	5.17	
Si VIII	316.215	7.60	0.60	3.47	
Mg VIII	317.028	2.80	0.59	1.39	
Si VIII	319.840	11.40	0.60	5.16	
Unid.	322.695	0.55	0.16	0.30	
Unid.	326.357	0.79	0.15	0.39	
Al VIII	328.249	1.72	0.18	0.79	
Al X	332.785	5.65	0.18	2.55	
Fe XIV	334.174	3.20	0.17	1.45	
Fe XVI	335.407	7.95	0.18	3.58	Bl. Mg VIII 335.231
Unid.	337.256	0.73	0.17	0.37	
Fe XII	338.260	2.13	0.25	0.99	
Mg VIII	338.995	3.34	0.22	1.52	
Fe XI	341.152	3.75	0.22	1.70	
Si IX	341.952	4.54	0.20	2.05	
Si IX	345.104	10.23	0.26	4.60	
Fe X	345.716	5.57	0.22	2.52	
Fe XII	346.858	2.67	0.24	1.22	
Si X	347.402	11.08	0.23	4.99	
Fe XIII	348.148	3.25	0.20	1.48	

Table 2—Continued

Ion	λ_{ref} Å	Flux	Stat. σ	Total σ	Remarks
		10^7 ph cm^{-2} s^{-1}			
Fe XI	349.148	1.18	0.19	0.56	Bl. Mg VI 349.108–349.179
Si IX	349.856	8.00	0.20	3.61	
Fe XII	352.111	6.77	0.61	3.11	Bl. Mg V 352.197, Al VII 352.159
Fe XI	352.671	8.90	0.60	4.05	
Si X	356.037	7.33	0.49	3.33	
Fe XI	358.656	2.90	0.53	1.41	Bl. Ne IV 358.688, 358.746
Fe XIII	359.777	3.40	0.61	1.64	Bl. Ne V 359.375
Fe XVI	360.798	1.62	0.40	0.83	
Fe XII	364.467	8.57	0.47	2.19	
Mg VII	365.179	2.10	0.60	0.80	
Fe X	365.553	2.48	0.60	0.86	Bl. Ne V 365.599
Mg VII	367.680	5.90	0.69	1.63	
Mg IX	368.059	49.35	0.58	12.35	
Fe XI	369.183	1.56	0.25	0.46	
O III	374.097	1.61	0.31	0.79	
He I	515.627	1.75	0.27	0.52	
Si XII	520.685	2.22	0.26	0.61	
He I	522.203	3.09	0.26	0.82	
O III	525.801	4.07	0.26	1.05	
He I	537.024	9.55	0.05	1.43	
O II	538.299	3.14	0.08	0.48	Bl. C III 538.312
O II	539.631	1.71	0.14	0.29	Bl. O II 539.086

Table 2—Continued

Ion	λ_{ref} Å	Flux	Stat. σ	Total σ	Remarks
		10^7 ph cm^{-2} s^{-1}			
Ne IV	541.116	0.46	0.05	0.08	
Ne IV	542.072	1.03	0.05	0.16	
Ne IV	543.881	1.90	0.05	0.29	
Al XI	550.050	1.43	0.16	0.27	
Unid.	551.348	0.37	0.18	0.18	
O IV	553.343	7.31	0.41	1.17	
O IV	554.512	35.59	0.37	5.35	Bl. O IV 554.076
O IV	555.270	4.41	0.18	0.69	
Ca X	557.764	2.98	0.18	0.48	
Ne VI	558.606	2.68	0.18	0.44	Bl. Ne VII 558.60
Ne VII	559.985	0.40	0.18	0.19	
Ne VII	561.725	1.36	0.18	0.27	
Ne VI	562.802	4.28	0.16	0.66	Bl. Ne VII 562.98
Ne VII	564.568	0.82	0.21	0.24	
Unid.	566.496	0.37	0.16	0.17	
Al XI	568.359	1.60	0.16	0.29	Bl. Ne V 568.421, Fe XV 2×284.147
Ne V	569.820	1.73	0.15	0.30	
Ne V	572.311	2.29	0.24	0.42	
Ca X	574.052	2.20	0.25	0.42	
Si XI	580.905	2.14	0.25	0.41	
He I	584.340	104.11	0.24	15.62	
Ar VII	585.694	1.33	0.31	0.37	

Table 2—Continued

Ion	λ_{ref} Å	Flux	Stat. σ	Total σ	Remarks
			10^7 ph cm^{-2} s^{-1}		
Unid.	592.501	1.12	0.27	0.39	
O III	597.823	0.46	0.09	0.15	Bl. Ca VIII 597.851
O III	599.596	10.97	0.10	2.74	
Si XI	2×303.351	40.81	3.51	8.88	
He II	2×303.780	678.41	4.11	135.74	
O IV	608.312	4.95	0.15	1.25	
Mg X	609.786	34.54	0.09	8.64	Bl. O IV 609.829
O II	616.309	0.91	0.11	0.26	
O IV	617.034	0.89	0.11	0.25	Bl. O II 617.063
Si X	621.11	0.55	0.47	0.49	Bl. K IX 621.436
Mg X	624.939	15.68	0.33	3.93	
O V	629.735	86.49	0.30	21.62	

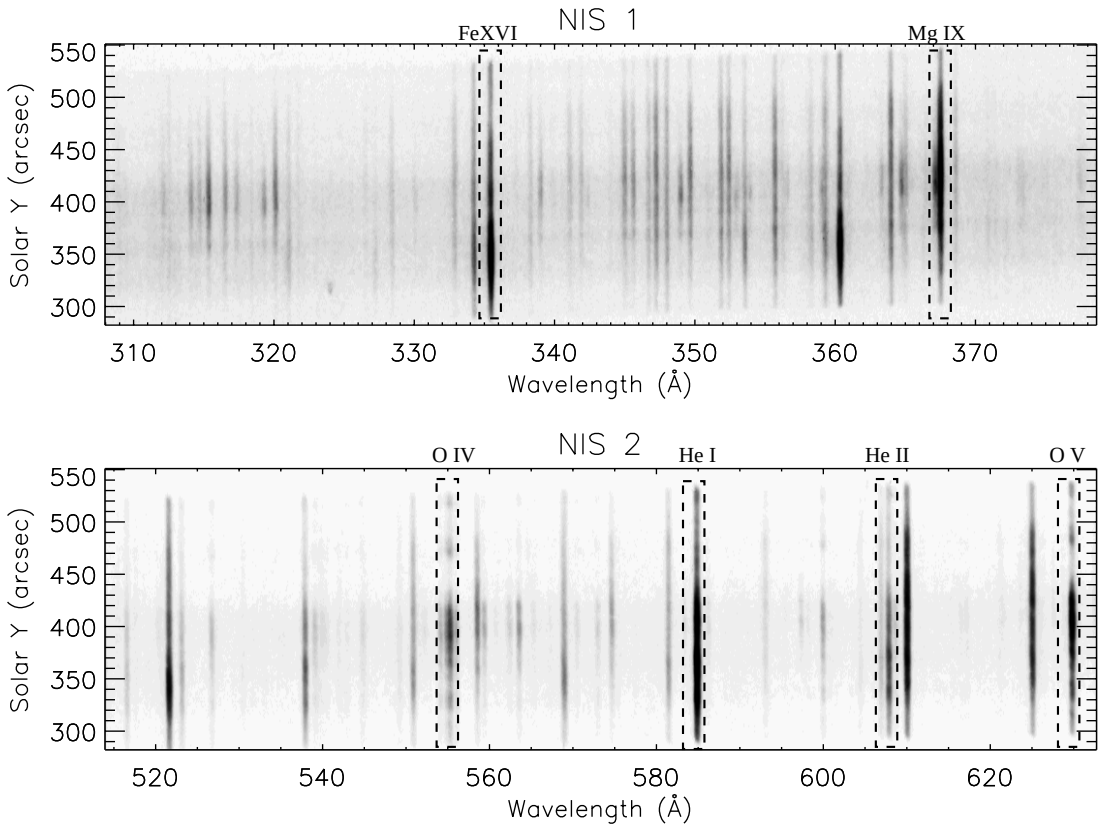

Fig. 1.— The NIS spectrum representing a 2 × 240 arcsec portion on the Sun as it appears on the face of the detector. The observation was made on March 14, 1997, 11:03 UT and the slit intercepted an active region. The line windows extracted from the detector when obtaining monochromatic full disk images are illustrated by the dashed boxes.

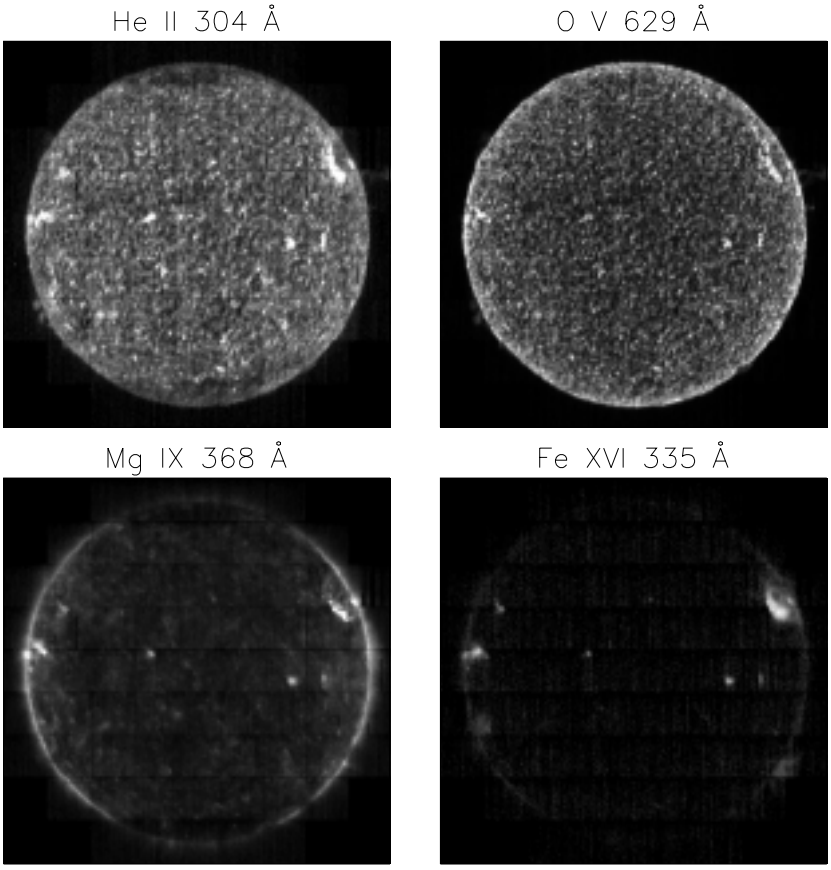

Fig. 2.— Monochromatic full disk images in 4 strong emission lines obtained with CDS on 16 May 1997. The network structure is clearly visible in He II 304 Å (6×10^4 K), and O V 629 Å (2.5×10^5 K), while in the Mg IX 368 Å (9.5×10^5 K) image the network pattern is less apparent. In the Fe XVI 335 Å ((2.5×10^6 K) image the emission comes from the active regions and bright compact regions. The Fe XVI line is displayed logarithmically, while the rest are linearly displayed.

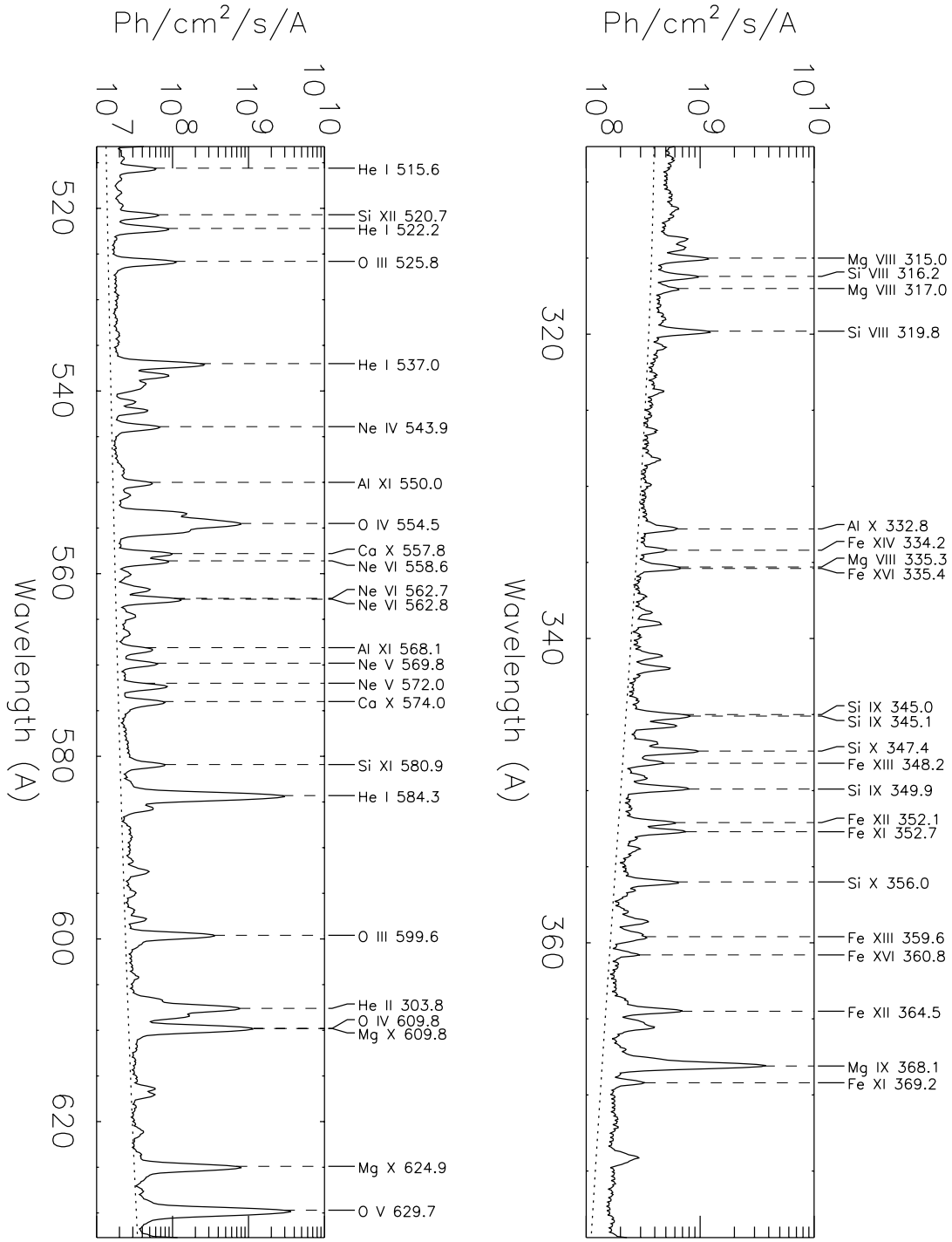

Fig. 3.— The "Sun as a Star" spectrum observed with the CDS Normal Incidence Spectrometer on 15 May 1997. The identification of most of the brightest lines are shown. Superimposed as a dotted line in each graph is the effect that a constant background would have on the two spectra, after passing through the calibration process. The interpretation is that the apparent background in the CDS/NIS data is dominated by off-band scattering.

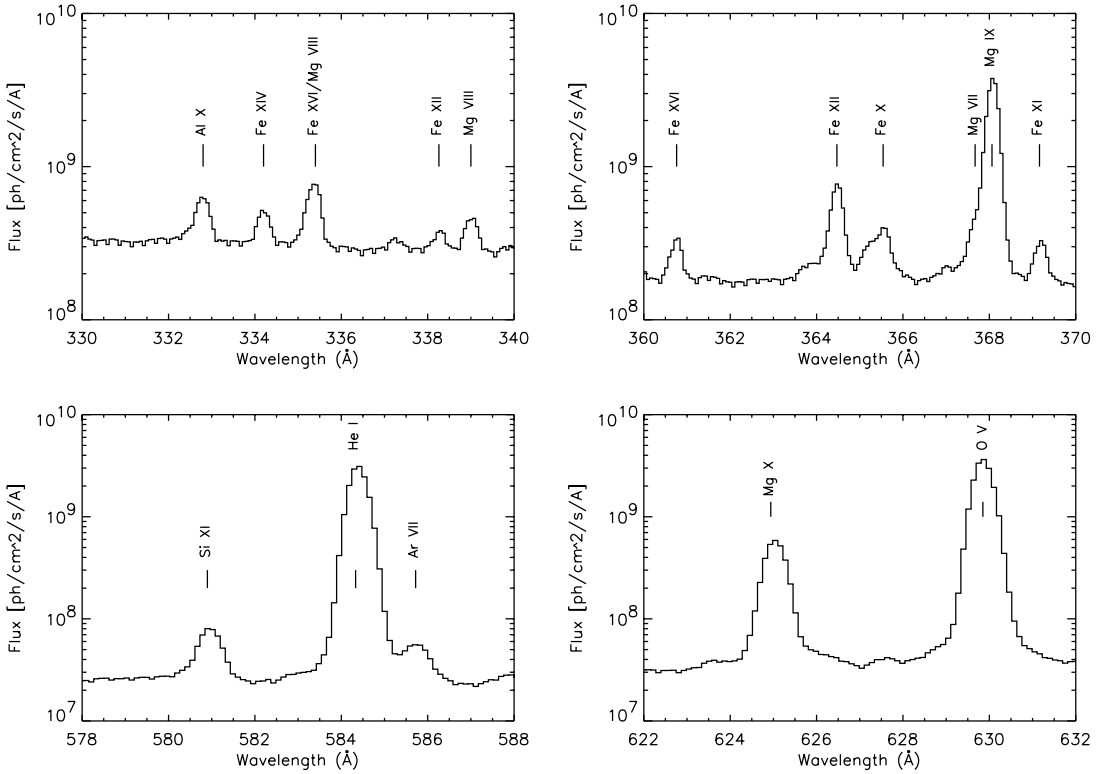

Fig. 4.— Four expanded wavelength plots to illustrate the high resolution of this irradiance spectrum obtained with CDS

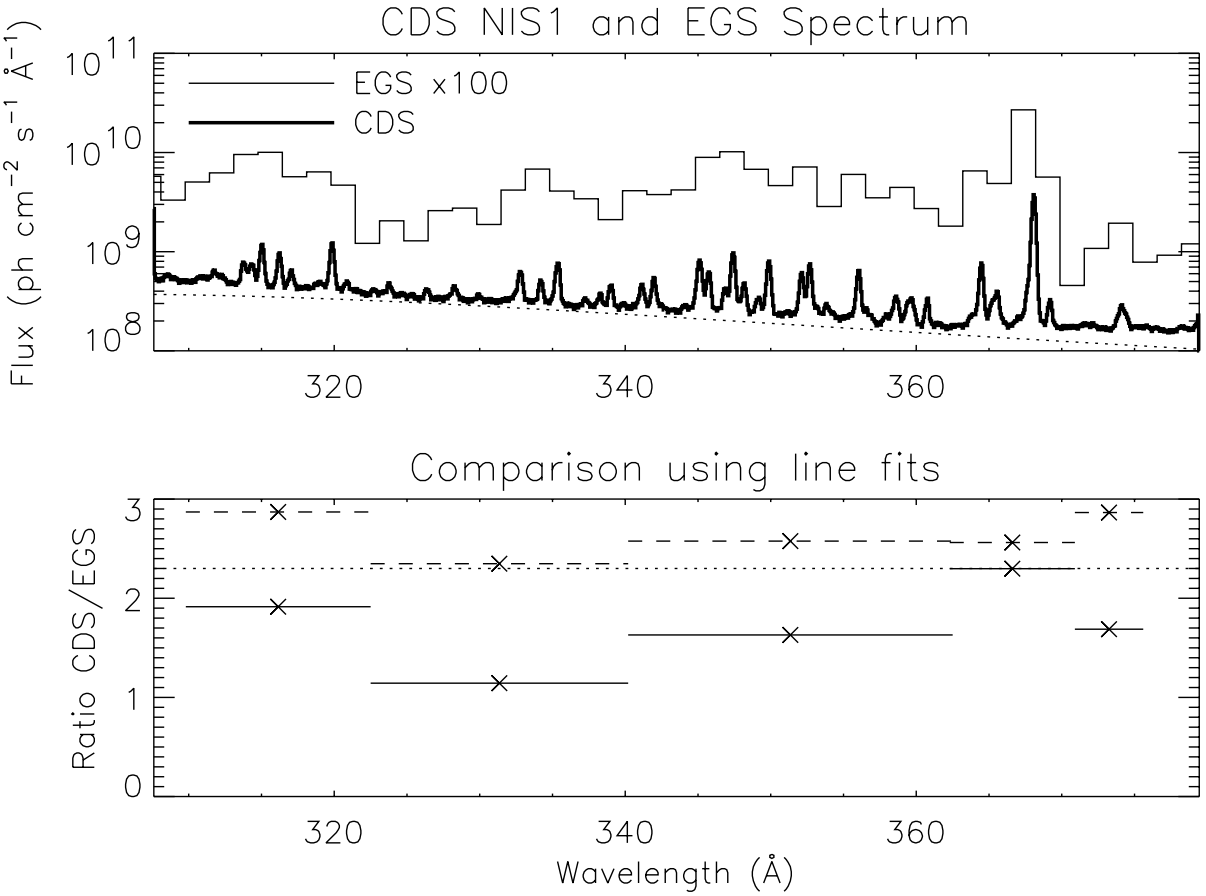

Fig. 5.— Upper panel: The full Sun NIS1 spectrum (bold line) compared with irradiance observations obtained with the EGS rocket experiment (narrow line) on May 15, 1997. The EGS spectrum has been multiplied by 100 for ease of display. The dotted line represents a theoretical model for off-band scattered light in the NIS spectrograph. Lower panel: The ratios of the irradiances measured by CDS to those measured by EGS. The solid lines represent no extra background subtraction for the EGS data, and the dashed lines represent the maximum possible background subtraction. The X symbols show the center wavelengths for each range analyzed. A constant ratio of 2.3 is represented by the dotted line.

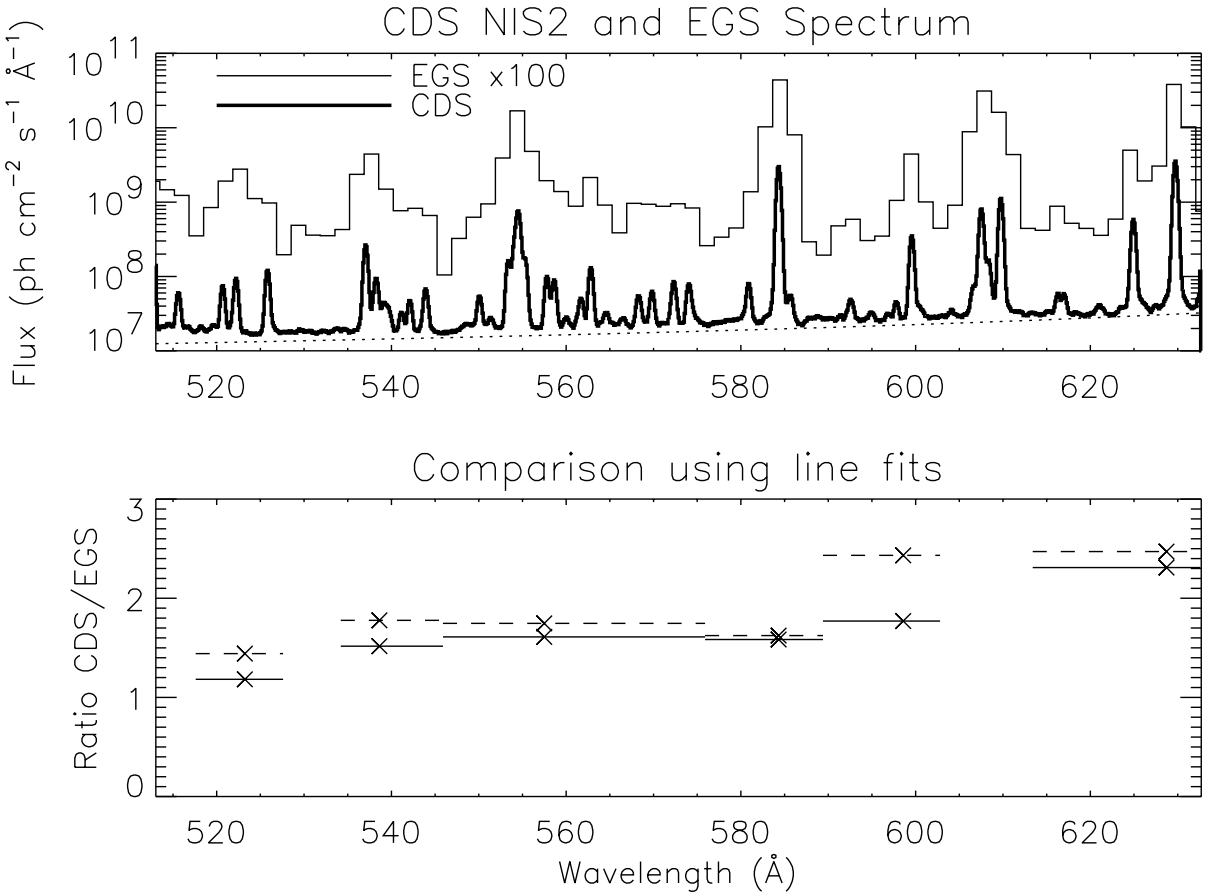

Fig. 6.— Upper panel: The full Sun NIS2 spectrum (bold line) compared with irradiance observations obtained with the EGS rocket experiment (narrow line) on May 15, 1997. The EGS spectrum has been multiplied by 100 for ease of display. The dotted line represents a theoretical model for off-band scattered light in the NIS spectrograph. Lower panel: The ratios of the irradiances measured by CDS to those measured by EGS. The solid lines represent no extra background subtraction for the EGS data, and the dashed lines represent the maximum possible background subtraction. The X symbols show the weighted average wavelengths for each range analyzed.

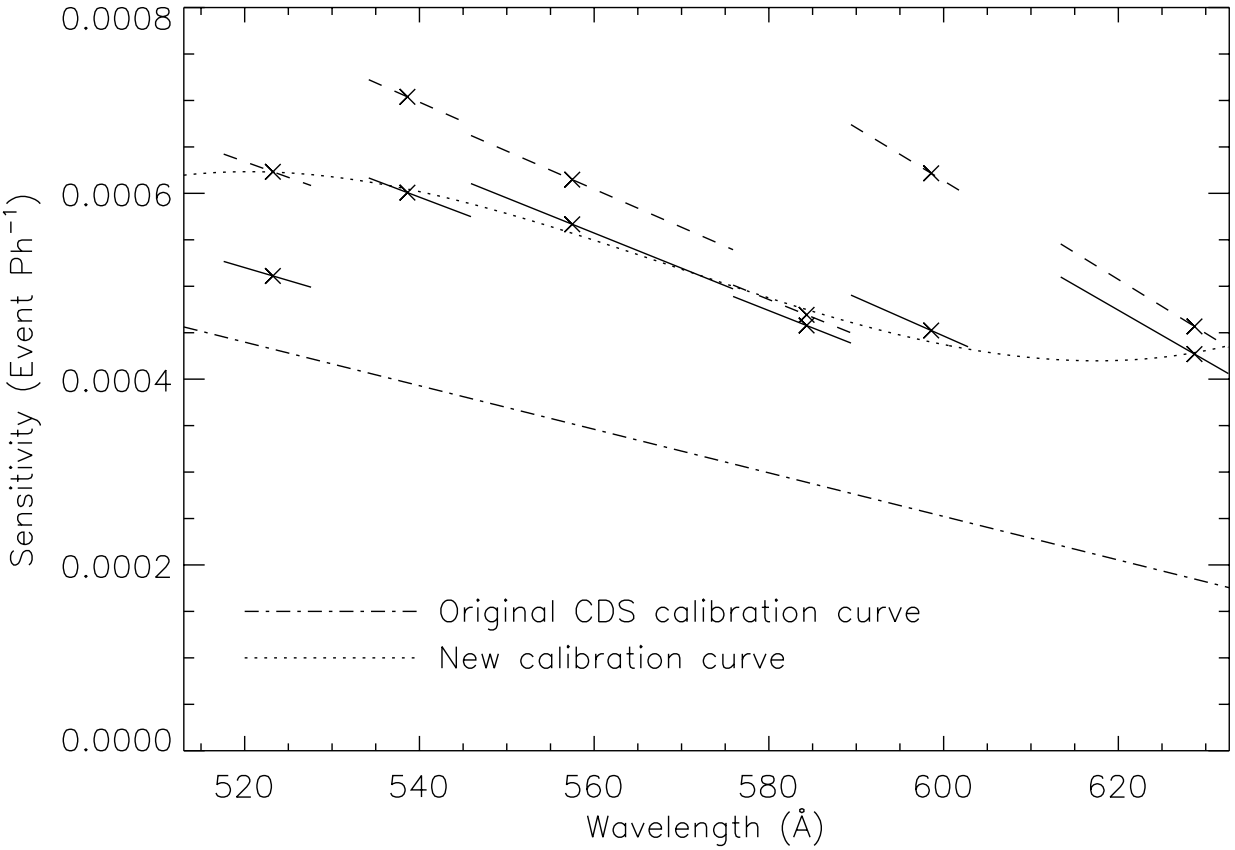

Fig. 7.— The correction factor to the CDS NIS2 sensitivity derived from the comparison with the EGS rocket data. The solid and dashed lines, and the X symbols, have the same meaning as in Fig. 6. The dot-dashed line is the original calibration curve, and the dotted curve is the new calibration curve based on the CDS and EGS comparison.

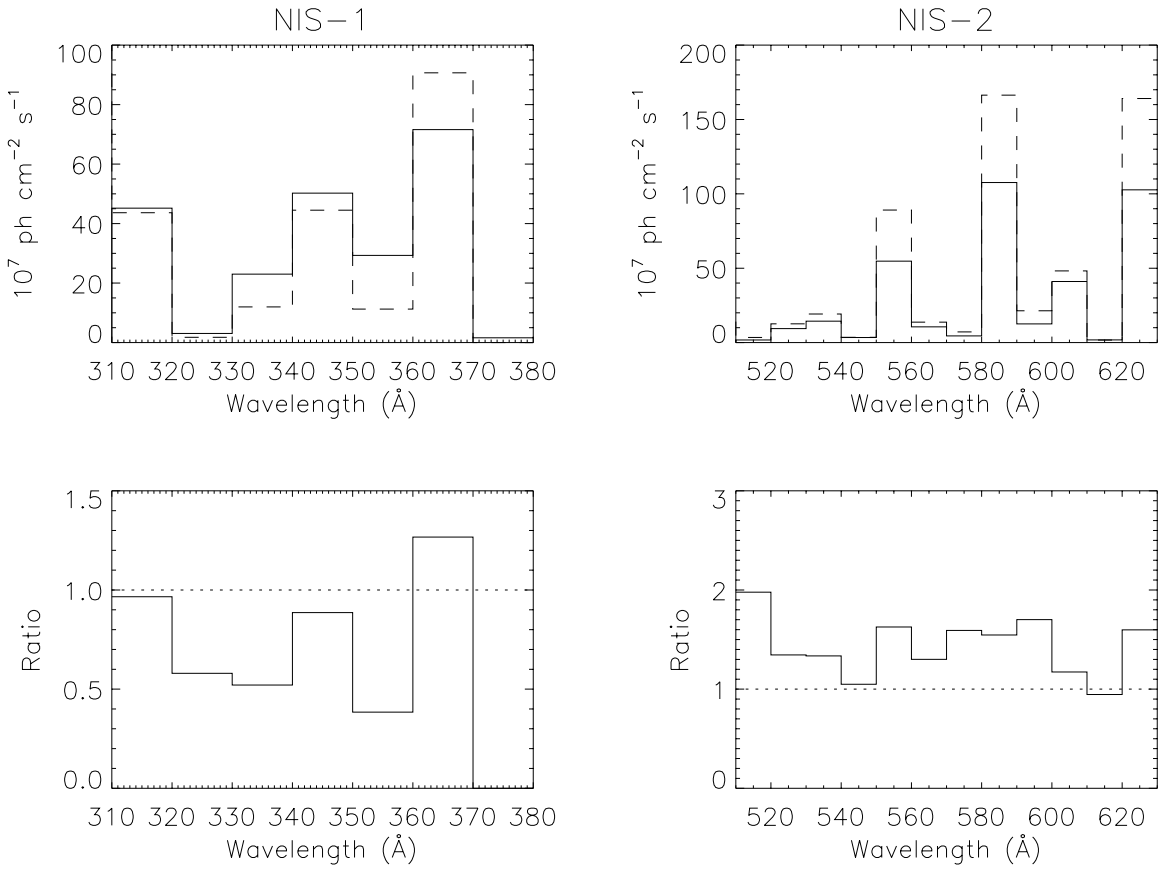

Fig. 8.— Comparison of the solar EUV irradiances measured by CDS to those predicted by the Hinteregger et al. (1981) model. In the upper plots, the solid lines represent the irradiances measured by CDS, while the dashed lines represent those predicted by the model. The data are binned into 10 Å bins to ease comparisons. In the lower plots, the solid lines show the ratio of the model predictions to the measurements, while unity is shown with a dotted line. The differences between the model and measured data are consistent with previous measurements by Woods et al. (1998).

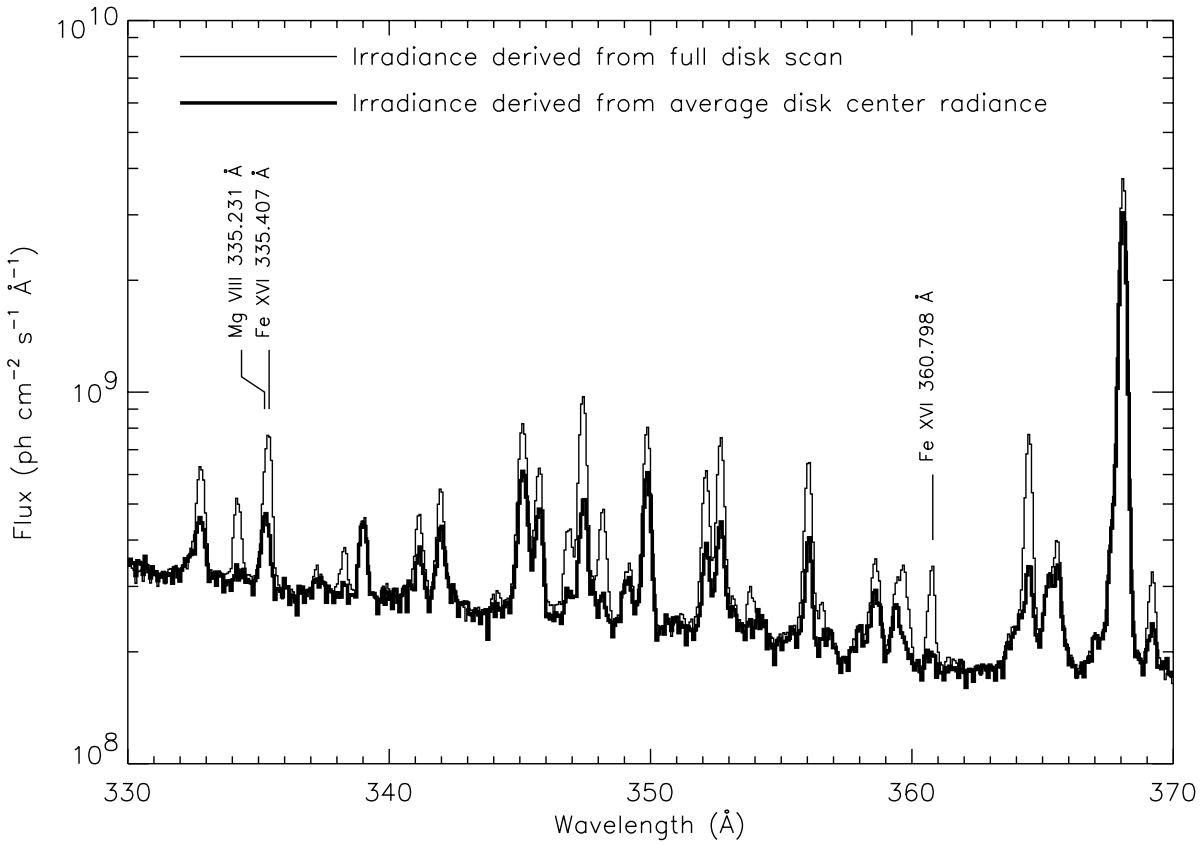

Fig. 9.— The full Sun spectrum (thin solid line) compared with irradiance values derived from the average quiet radiance at disk center (thick solid line). The latter was derived from the raster centered on the solar disk using equation 1. The coronal lines are obviously weaker, or even absent in the average quiet Sun spectrum.